RAC1 Missense Mutations in Developmental Disorders with Diverse Phenotypes

Margot R.F. Reijnders,[1,15] Nurhuda M. Ansor,[2,3,15] Maria Kousi,[4,15] Wyatt W. Yue,[5] Perciliz L. Tan,[4] Katie Clarkson,[6] Jill Clayton-Smith,[7,8] Ken Corning,[6] Julie R. Jones,[6] Wayne W.K. Lam,[9] Grazia M.S. Mancini,[10] Carlo Marcelis,[1] Shehla Mohammed,[11] Rolph Pfundt,[1] Maian Roifman,[12,13] Ronald Cohn,[13] David Chitayat,[12,13] Deciphering Developmental Disorders Study, Tom H. Millard,[2] Nicholas Katsanis,[4] Han G. Brunner,[1,14,*] and Siddharth Banka[7,8,*]

RAC1 is a widely studied Rho GTPase, a class of molecules that modulate numerous cellular functions essential for normal development. RAC1 is highly conserved across species and is under strict mutational constraint. We report seven individuals with distinct *de novo* missense *RAC1* mutations and varying degrees of developmental delay, brain malformations, and additional phenotypes. Four individuals, each harboring one of c.53G>A (p.Cys18Tyr), c.116A>G (p.Asn39Ser), c.218C>T (p.Pro73Leu), and c.470G>A (p.Cys157Tyr) variants, were microcephalic, with head circumferences between −2.5 to −5 SD. In contrast, two individuals with c.151G>A (p.Val51Met) and c.151G>C (p.Val51Leu) alleles were macrocephalic with head circumferences of +4.16 and +4.5 SD. One individual harboring a c.190T>G (p.Tyr64Asp) allele had head circumference in the normal range. Collectively, we observed an extraordinary spread of ∼10 SD of head circumferences orchestrated by distinct mutations in the same gene. In silico modeling, mouse fibroblasts spreading assays, and *in vivo* overexpression assays using zebrafish as a surrogate model demonstrated that the p.Cys18Tyr and p.Asn39Ser RAC1 variants function as dominant-negative alleles and result in microcephaly, reduced neuronal proliferation, and cerebellar abnormalities *in vivo*. Conversely, the p.Tyr64Asp substitution is constitutively active. The remaining mutations are probably weakly dominant negative or their effects are context dependent. These findings highlight the importance of *RAC1* in neuronal development. Along with TRIO and HACE1, a sub-category of rare developmental disorders is emerging with RAC1 as the central player. We show that ultra-rare disorders caused by private, non-recurrent missense mutations that result in varying phenotypes are challenging to dissect, but can be delineated through focused international collaboration.

Developmental disorders (DDs) are etiologically extremely heterogeneous and affect 2%–5% of individuals.[1,2] *De novo* mutations account for a substantial proportion of DDs and are thought to underlie approximately 400,000 new DD-affected case subjects world-wide annually.[3] Recently, large-scale next generation sequencing studies have led to the identification of several DD-associated genes that lead to clinical manifestations through protein truncating or recurrent missense variants.[4–6] However, rare disorders caused by private, non-recurrent missense mutations that result in varying phenotypes remain challenging to dissect.[7]

Several human DDs are known to result from mutations in members of the RAS superfamily of small GTPases.[8] The RAS superfamily is further divided into smaller families, one of which is the 22-member Rho family. Rho GTPases cycle between active GTP-bound and inactive GDP-bound states. Their activity is regulated by guanine nucleotide exchange factors (GEFs), GTPases activating proteins (GAPs), and guanine nucleotide dissociated inhibitors (GDIs).[9] Rho GTPases modulate essential cellular functions, including cell polarity, migration, vesicle trafficking, and cytokinesis and play crucial roles in neuronal development, neuronal survival, and neurodegeneration.[10–12] However, no human DDs caused by mutations in genes encoding Rho GTPases are known.

One of the most widely studied Rho GTPases is the RAS-related C3 Botulinum Toxin Substrate 1 (RAC1).[13] RAC1 is part of the RAC Rho GTPases subfamily that also includes RAC2, RAC3, and RhoG.[14] RAC1 is an important modulator of the cytoskeleton, with a critical function in phagocytosis, mesenchymal-like migration, neuronal polarization, axonal growth, adhesion, and differentiation of multiple cell types.[10,15,16] Additionally, it is involved in

[1]Department of Human Genetics, Radboud University Medical Center, 6500 HB Nijmegen, the Netherlands; [2]Division of Developmental Biology & Medicine, Faculty of Biology, Medicine and Health, University of Manchester M13 9PL, UK; [3]Advanced Medical and Dental Institute, Universiti Sains Malaysia, Bertam, 13200 Kepala Batas, Penang, Malaysia; [4]Center for Human Disease Modeling, Department of Cell Biology, Duke University, Durham, NC 27701, USA; [5]Structural Genomics Consortium, Nuffield Department of Medicine, University of Oxford, Oxford OX3 7DQ, UK; [6]Greenwood Genetic Center, Greenwood, SC 29646, USA; [7]Manchester Centre for Genomic Medicine, St. Mary's Hospital, Central Manchester NHS Foundation Trust, Manchester Academic Health Sciences Centre, Manchester M13 9WL, UK; [8]Division of Evolution and Genomic Sciences, Faculty of Biology, Medicine and Health, University of Manchester, Manchester M13 9PL, UK; [9]South East of Scotland Clinical Genetic Service, Western General Hospital, Edinburgh EH4 2XU, UK; [10]Department of Clinical Genetics, Erasmus Medical Center, 3000 CA Rotterdam, the Netherlands; [11]Department of Clinical Genetics, Guy's and St Thomas' Hospital, London SE1 7EH, UK; [12]The Prenatal Diagnosis and Medical Genetics Program, Department of Obstetrics and Gynecology, Mount Sinai Hospital, Toronto, ON M5G 1X5, Canada; [13]Division of Clinical and Metabolic Genetics, Department of Paediatrics, The Hospital for Sick Children, University of Toronto, Toronto, ON M5G 1X8, Canada; [14]Department of Clinical Genetics and School for Oncology & Developmental Biology (GROW), Maastricht University Medical Center, 6202 AZ Maastricht, the Netherlands
[15]These authors contributed equally to this work
*Correspondence: han.brunner@radboudumc.nl (H.G.B.), siddharth.banka@manchester.ac.uk (S.B.)
http://dx.doi.org/10.1016/j.ajhg.2017.08.007.

cellular growth and cell-cycle regulation via mTOR signaling.[17] In mouse studies, Rac1 is required for the formation of three germ layers during gastrulation, with *Rac1*-knockout mice being embryonic lethal.[18] Conditional forebrain-specific *Rac1*-knockout mice display impaired neuronal migration, abnormal dendritic growth and remodelling, disruption of lamellipodia formation, reduced neuronal proliferation, premature differentiation, and microcephaly.[19–21] Here, we report *de novo* missense *RAC1* (MIM: 602048) mutations in individuals with DD and divergent phenotypes.

All procedures followed were in accordance with the ethical standards of the institutional and national responsible committees on human or animal experimentation and that, where relevant, informed consent was obtained. Review of data from 4,293 families, who underwent trio whole-exome sequencing (WES) as part of the Deciphering Developmental Disorders study,[3] led to identification of three individuals with *de novo RAC1* (GenBank: NM_006908) missense mutations: individual 3 with c.218C>T (p.Pro73Leu), individual 5 with c.190T>G (p.Tyr64Asp), and individual 6 with c.151G>A (p.Val51Met) (Table 1; Figures 1 and 2). Two additional individuals were independently ascertained through family-based diagnostic WES: individual 1 with c.53G>A (p.Cys18Tyr) and individual 2 with c.116A>G (p.Asn39Ser) (Table 1; Figures 1 and 2). While functional studies were ongoing for the five individuals, two additional individuals were identified via the GeneMatcher tool[22] or through international collaboration: individual 4 with c.470G>A (p.Cys157Tyr) and individual 7 with c.151G>C (p.Val51Leu) (Table 1; Figures 1 and 2).

Human *RAC1* (ENSG00000136238) encodes six transcripts, of which two are protein coding: RAC1 and RAC1B (Figure 1A). Of the two protein-coding transcripts, GenBank: NM_006908 (RAC1, ENST00000348035.8) lacks exon 4 and encodes the shorter RAC1 isoform of 192 amino acids, which is ubiquitously expressed in all tissues.[23] *RAC1* is under strict mutational constraint with only 15 missense variants observed versus 75.9 expected in ~60,000 exomes cataloged in the ExAC database (z-score = 3.42).[24] Moreover, 7 of these 15 observed missense variants are located in exon 4, which is included only in RAC1B (ENST00000356142.4) that encodes the longer isoform and is mainly expressed in gastrointestinal and epithelial tissues.[25] Of particular note, there are no missense variants in exons 1, 2, 3, and 5 in the ExAC database (Figure 1B). Six out of seven mutations described here are in exons 2 and 3. The p.Cys157Tyr change (p.Cys176Tyr in the longer RAC1B) lies in a sub-region of exon 7 with no known germline human missense variants (Figure 1B). None of the identified mutations were present in any of the in-house variant databases of the four centers participating in this study. All six amino acids affected by the seven mutations are highly conserved among different species (Figure 1C). All reported *RAC1* mutations are within or in proximity to G box residues and/or conserved residues present in 90% of the RAS superfamily members (Figure 1C).[26] Collectively, the genetic data were strongly supportive of deleteriousness for each of the seven mutations.

Informed consent for publication of photographs was obtained from legal guardians. Detailed clinical information was collected on all affected individuals (Table 1; Figure 2; see Supplemental Note). All seven individuals (age range 4.5 months–15 years) had moderate to severe intellectual disability (ID) and variable degrees of neurological involvement including hypotonia (4/7), epilepsy (3/7), behavioral problems (3/7), and stereotypic movements (2/7). However, their occipital frontal circumferences (OFC) were remarkably different: individuals 1, 2, 3, and 4 were microcephalic (OFCs of −2.5, −3, −5, and −2.5 SD, respectively), individual 5 with p.Tyr64Asp mutation had a normal OFC (+1 SD), and individuals 6 and 7, both with mutations affecting Val51, were macrocephalic (OFCs of +4.16 and +4.5 SD, respectively) (Table 1; Figure 2). Hypoplasia of the corpus callosum and the cerebellar vermis were the commonest features observed on available magnetic resonance imaging (MRI) studies of individuals with microcephaly. However, they all had additional abnormalities (Supplemental Note; Figure 2). Individual 5 (with normal OFC) was reported to have polymicrogyria and hypoplastic corpus callosum (images not available). The two individuals with macrocephaly (individuals 6 and 7) showed periventricular white matter lesions (Table 1; Figure 2). Arched eyebrows, dysplastic ears, prominent nasal bridges, and overhanging columellae were shared between a majority of individuals without macrocephaly (Supplemental Note; Figure 2), but their facial dysmorphism does not overlap sufficiently to make this condition recognizable via their gestalt. Both individuals with macrocephaly displayed prominent broad foreheads, open mouth appearance, and scooped out appearance on lateral view (Figure 2). Collectively, the clinical data suggested a remarkable phenotypic variability in our cohort.

We mapped each of the seven identified mutations onto the available crystal structure of human RAC1 (PDB: 3TH5) (Figure 1D) to gain insights into their effect on the protein structure and function. The amino acids affected by the seven mutations could be categorized into three groups. (1) Cys18 and Cys157 are located in and adjacent to, respectively, the guanine nucleotide binding site that binds GTP/GDP. These two cysteine thiols can be oxidized by glutathionylation, a post-translational modification that alters GTP binding and exchange activities of RAC1.[27] The p.Cys18Tyr and p.Cys157Tyr substitutions introduce a bulky aromatic residue in place of the thiol group and are expected to impact GTPase activity either by directly interfering with GTP binding or indirectly by abolishing the post-translational modification. (2) Asn39 is part of the switch I motif, while Tyr64 and Pro73 are within and adjacent to, respectively, the switch II motif. Both switch motifs are highly conserved regions involved

Table 1. RAC1 Mutations and Phenotype

	Individual 1	Individual 2	Individual 3	Individual 4	Individual 5	Individual 6	Individual 7
	microcephaly	microcephaly	microcephaly	microcephaly	normal OFC	macrocephaly	macrocephaly
Gender	male	male	male	male	male	male	male
Ethnicity	European/Egyptian	European	European	European/Armenian	European/Asian	European	African American
Age at examination	13 years	9 years	15 years	4.5 months	12 years	33 months	4 years 5 months
Mutation (GenBank: NM_006908)							
Chromosome position (Hg19)	chr7:6426860G>A	chr7:6431563A>G	chr7:6431665C>T	chr7:6441968G>A	chr7:643163T>G	chr7:6431598G>A	chr7:6431598G>C
cDNA change	c.53G>A	c.116A>G	c.218C>T	c.470G>A	c.190T>G	c.151G>A	c.151G>C
Amino acid change	p.Cys18Tyr	p.Asn39Ser	p.Pro73Leu	p.Cys157Tyr	p.Tyr64Asp	p.Val51Met	p.Val51Leu
Likely effect of the mutation	dominant negative	dominant negative	unknown	unknown	constitutively active	unknown	unknown
Growth							
Height	127 cm (−2.5 SD)	128 cm (−2.5 SD)	unknown	62 cm (−1 SD)	134 cm (+1.03 SD) (8 years)	unknown	109 cm (0 SD)
Weight	30 kg (0 SD)	24 kg (−0.5 SD)	unknown	4.8 kg (−3 SD)	unknown	unknown	23 kg (+2.5 SD)
Head circumference	50 cm (−2.5 SD)	47.7 cm (−3 SD)	47 cm (−5 SD)	39 cm (−2.5 SD)	56.5 cm (+1 SD)	57 cm (+4.16 SD)	59.5 cm (+4.5 SD)
Development							
Intellectual disability	yes	yes	yes	yes	yes	yes	yes
Mild/Moderate/Severe	moderate	mild-moderate	severe	unknown	severe	moderate	unknown
Neurological							
Epilepsy	yes	no	unknown	yes	no	unknown	yes
Hypotonia	yes	no	unknown	yes	yes	unknown	yes
Behavioral problems	no	yes - hyperactive	unknown	unknown	yes - sleep disturbances	unknown	yes - autism
Stereotypic movements	no	no	unknown	no	yes	unknown	yes
Brain MRI Abnormalities							
Cerebellar abnormalities	yes	yes	unknown	yes	no	no	no
Hypoplasia corpus callosum	yes	yes	unknown	yes	yes	no	no
Enlarged lateral ventricles	yes	yes	unknown	no	no	no	no
Enlarged fourth ventricle	no	yes	unknown	no	no	no	no
Thin pons brain stem	no	yes	unknown	yes	no	no	no
Mega cisterna magna	yes	yes	unknown	yes	no	no	no

(*Continued on next page*)

Table 1. *Continued*

	Individual 1	Individual 2	Individual 3	Individual 4	Individual 5	Individual 6	Individual 7
	microcephaly	microcephaly	microcephaly	microcephaly	normal OFC	macrocephaly	macrocephaly
Polymicrogyria	no	no	unknown	no	yes	no	no
White matter lesions	yes	no	unknown	no	no	yes	yes
Congenital Abnormalities							
Cardiac abnormalities	yes – NS LVC; IV	no	unknown	yes – PDA, PFO, BAV	yes - VSD	unknown	no
Hypospadias	no	no	unknown	yes	yes	unknown	no
Other							
Neonatal feeding difficulties	yes	yes	yes	no	no	unknown	no
Other	plagiocephaly; scoliosis; small hands and feet; hyperlaxity; brachydactyly 5th digit; SC bilateral	recurrent pneumonias; eczema	diabetes mellitus	umbilical hernia, tracheobronchomalacia; cryptorchidism	mild visual impairment; congenital sensorineural hearing impairment; abnormal creases in hands	none	non-verbal; recurrent otitis media; eczema

Abbreviations are as follows: BAV, bicuspid aortic valve; IV, insufficiency all valves; NS LVC, non-synchronic left ventricle contractions; PDA, patent ductus arteriosus; PFO, patent foramen ovale; SC, simian crease; VSD, ventricular septum defect.

in the interactions with various GEFs and GAPs (e.g., Rex1, DOCK),[28] mediating the conformational changes for guanine nucleotide exchange (Figure S1), and downstream effectors. Missense mutations affecting these residues are likely to impact the protein-protein interactions directly. (3) Val51 has no obvious involvement in GTP binding or interactions with GEF/GAPs. Free energy calculations by FoldX (in the SNPeffect 4.0 server)[29] revealed a reduction of protein stability for these two substitutions (ΔΔG of 2.13 and 1.94 kcal/mol for p.Val51Met and p.Val51Leu, respectively).

RAC1 is known to regulate the spreading of fibroblasts plated onto fibronectin.[30] The genetic data and in silico modeling suggested that the phenotypes are unlikely to result from haploinsufficiency. We reasoned that the *RAC1* mutations identified in this study could be dominant negative or acting as constitutively active. If so, these mutations should result in changes in fibroblast spreading. To test this hypothesis, we introduced selected *RAC1* mutations in NIH 3T3 fibroblasts. Mammalian expression plasmids encoding GFP-Rac1, GFP-Rac1-T17N, and GFP-Rac1-Q61L were obtained from Prof. Viki Allan (Manchester). A Quikchange Lightning kit (Agilent Technologies) was used to introduce point mutations in the GFP-Rac1 expression plasmid. We generated plasmids encoding 6/7 variants identified in this study (p.Cys18Tyr, p.Asn39Ser, p.Val51Met, p.Tyr64Asp, p.Pro73Leu, and p.Cys157Tyr) along with p.Thr17Asn that is known to have a dominant-negative effect[31] and p.Gln61Leu which is known to result in constitutive protein activation.[32] NIH 3T3 fibroblasts were cultured in a 24-well plate and were transfected with the Rac expression plasmids 24 hr after plating using Fugene 6 reagent (Promega). 48 hr after transfection, the fibroblasts were trypsinized then replated onto fibronectin-coated coverslips. 30 min after re-plating, the coverslips were rinsed with PBS and fixed with 4% paraformaldehyde (PFA). The fixed cells were then permeabilized with 0.1% Triton X-100 in PBS followed by blocking with 1% BSA in PBS. The cells were stained with a rabbit anti-GFP (Invitrogen) antibody (1:500), followed by an Alexa 488 anti-rabbit secondary antibody (Invitrogen) and Alexa568-phalloidin (Invitrogen) before mounting in Prolong Gold (Invitrogen). Cells were imaged on a Nikon A1R confocal microscope, using a 60× 1.4NA oil objective.

Cell circularity values were obtained using ImageJ software. Cell perimeters were identified using the ImageJ "threshold" function and then circularity index ($4\pi \times \text{area}/\text{perimeter}^2$) was calculated using the "analyze particles" function. Circularity datasets were statistically analyzed using one-way ANOVA with Dunnett's correction for multiple comparisons. At least 50 cells were analyzed for each dataset except p.Asn39Ser, p.Tyr64Asp, p.Cys157Tyr (>40 cells), and p.Gln61Leu (25 cells). Data were pooled from three independent experiments and highly expressing cells were excluded. Morphology was also assessed qualitatively by classifying cells according to their predominant actin protrusion type. Three

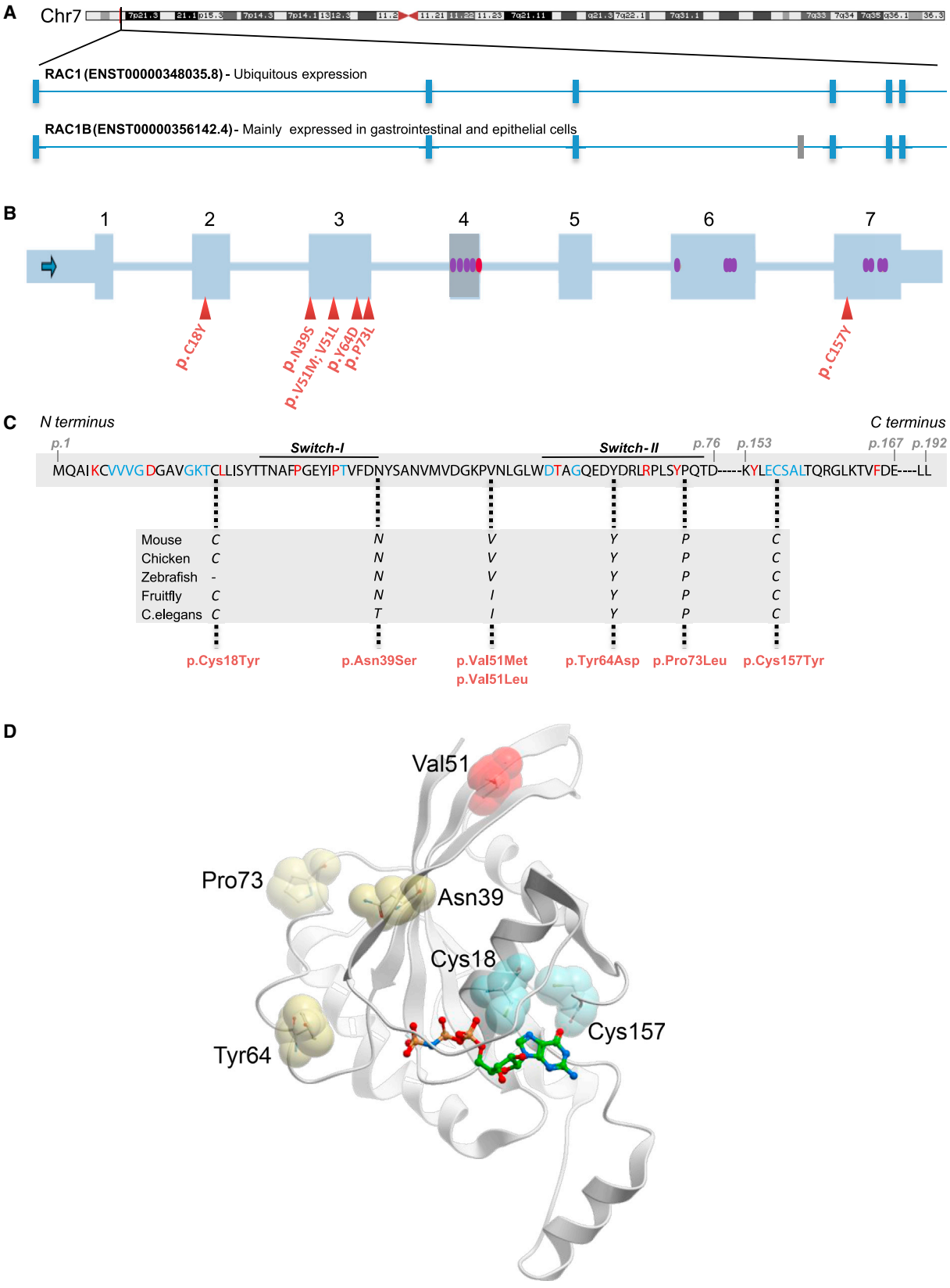

Figure 1. Properties of Germline *RAC1* Variants

(A) *RAC1* is located on human chromosome 7p22.1. Exon-intron structure of the two protein-coding *RAC1* transcripts is shown. The ubiquitously expressed *RAC1* transcript is composed of six exons (blue vertical lines). *RAC1B* (mainly expressed in gastrointestinal and epithelial cells) contains an additional exon (exon 4; gray vertical line).

(legend continued on next page)

categories were used: (1) >50% of cell perimeter occupied of filopodia, (2) >50% of perimeter occupied by lamellipodia/ruffles, and (3) mixed protrusions, with neither type occupying 50% of the perimeter.

The majority (51%) of cells transfected with wild-type Rac1 exhibited mixed protrusions, with the remaining cells split almost equally between those in which >50% the perimeter was occupied by filopodia or lamellipodia/ruffles (Figure 3A). As observed previously, transfection of the known dominant-negative p.Thr17Asn variant resulted in a filopodia-rich cell perimeter and a significantly reduced circularity index (Figures 3A–3C).[30] By contrast, expression of the known constitutively active p.Gln61Leu variant resulted in virtually all cells exhibiting large lamellipodia or membrane ruffles and a significantly increased circularity index.[33] Expression of the p.Cys18Tyr and p.Asn39Ser variants (seen in individuals 1 and 2 with microcephaly) resulted in a phenotype reminiscent of dominant-negative Rac1, with an increase in the proportion of cells rich in filopodia and a reduction in cells rich in lamellipodia/ruffles (Figures 3A and 3C). Consistently, these mutations exhibited a significantly decreased circularity index (Figure 3B). By contrast, cells transfected with the p.Tyr64Asp substitution resulted in a phenotype more reminiscent of constitutive active Rac1, with significantly increased circularity index and a greater proportion of cells exhibiting lamellipodia or ruffles (Figures 3A–3C). Cells expressing p.Val51Met, p.Pro73Leu, and p.Cys157Tyr all showed a tendency toward increased filopodia and reduced lamellipodia but did not result in a significant change in circularity index relative to cells expressing wild-type Rac, suggesting at most a modest impact on Rac function in these assays (Figures 3A–3C). All the Rac1 mutant proteins exhibited similar cellular localization to wild-type Rac1 with the exception of p.Tyr64Asp, which appeared to localize strongly to the leading edge of ruffles and lamellipodia (Figure 3C).

Next, we sought to explore the *in vivo* effects of *RAC1* mutations in zebrafish embryos. Toward this, we identified *rac1a* as the sole zebrafish ortholog with highest degree of homology to the human *RAC1* (90% similarity, 90% identity) and used the CRISPR/Cas9 system to introduce deletions, as a way to explore the phenotypic effects induced by loss of function of *RAC1*. Guide RNAs targeting the *Danio rerio* coding region of *rac1* were generated as previously described.[34,35] We observed sequence aberrations in 30% of the evaluated *rac1* clones (Figure S2A). Assessment of mosaic F0 embryos injected with a guide against exon 2 did not result in statistically different head size counts between F0 CRISPR and control embryos (Figure S2B). No overt morphological changes were observed in the genetically edited embryos.

We next considered a dominant effect of the *RAC1* alleles. To test this hypothesis, we cloned the human wild-type *RAC1* mRNA (GenBank: NM_018890) into the pCS2+ vector and transcribed *in vitro* using the SP6 Message Machine kit (Ambion). The mouse fibroblast spreading assays had indicated that dominant-negative effects could be a common mechanism for *RAC1* mutations. We therefore introduced the two variants (p.Cys18Tyr and p.Asn39Ser) that were shown to be the strongest genocopies of the known dominant-negative mutation using Phusion high-fidelity DNA polymerase (New England Biolabs) and custom-designed primers. Additionally, for sake of comparison, we also introduced the known dominant-negative (p.Thr17Asn) and constitutively active (p.Gln61Leu) mutants. Based on the dose-curve for the titration of the effect that WT *RAC1* had on the head-size phenotype (Figure S3), we injected 50 pg of WT or mutant RNA into wild-type zebrafish embryos at the 1- to 4-cell stage. The injected larvae were grown to 5 dpf and imaged live on dorsal view. The area of the head was traced excluding the eyes from the measurements and statistical significance was calculated using Student's t test. All experiments were repeated three times and scored blind to injection cocktail. Injection of RNA encoding p.Thr17Asn, p.Cys18Tyr, or p.Asn39Ser in zebrafish embryos induced a significant decrease in head-size ($p < 0.0005$) compared to controls (Figures 4A and 4B). Injection of RNA encoding p.Gln61Leu induced a significant increase in head-size ($p < 0.0001$) compared to controls (Figures 4A and 4B). Importantly, the head-size could not be rescued by co-injection of mutant *RAC1* with WT message (Figure S4) arguing further in favor of these *RAC1* mutations acting as dominant alleles *in vivo*, consistent with our results of mouse fibroblast spreading assay.

Driven by the fact that RAC1 is involved in neuronal proliferation,[20] we next assessed neuronal proliferation in the brain of embryos injected with WT or a subset of mutant *RAC1* (encoding p.Cys18Tyr or p.Asn39Ser). To do this, the injected embryos were fixed overnight at 48 hr post fertilization (hpf) in Dent's fixative (80%

(B) Schematic of *RAC1*, with the coding exons shown as blue rectangles and the introns as blue lines. Exon 4 that is expressed only in the longer *RAC1B* transcript is shown as a gray rectangle. The red triangles represent the positions of the mutations identified in this study. The red oval within exon 4 shows the two splice donor variants detected in the ExAC database. The purple ovals represent the missense variants in the ExAC database.
(C) Amino acid sequence of the RAC1 across positions p.1-p.192. Red amino acids are highly conserved in >90% of the RAS family members and blue amino acids represent RAS protein G box consensus residues. Positions of the identified missense mutations (in red) are marked with dotted lines and the high conservation among different species of these amino acids is shown in the rectangle below.
(D) Crystal structure of human RAC1 showing the position of the identified missense variants presented in this study. The sites of substitution are indicated by sticks in spheres and are color coded according to their putative impact on guanine nucleotide binding (cyan), protein-protein interactions (yellow), and structural stability (red). For reference, the non-hydrolyzable GTP analog GMPPNP bound to the structure is shown in sticks. The structure was analyzed and this figure was generated using the program ICM-Pro v3.8 (Molsoft, LLC).

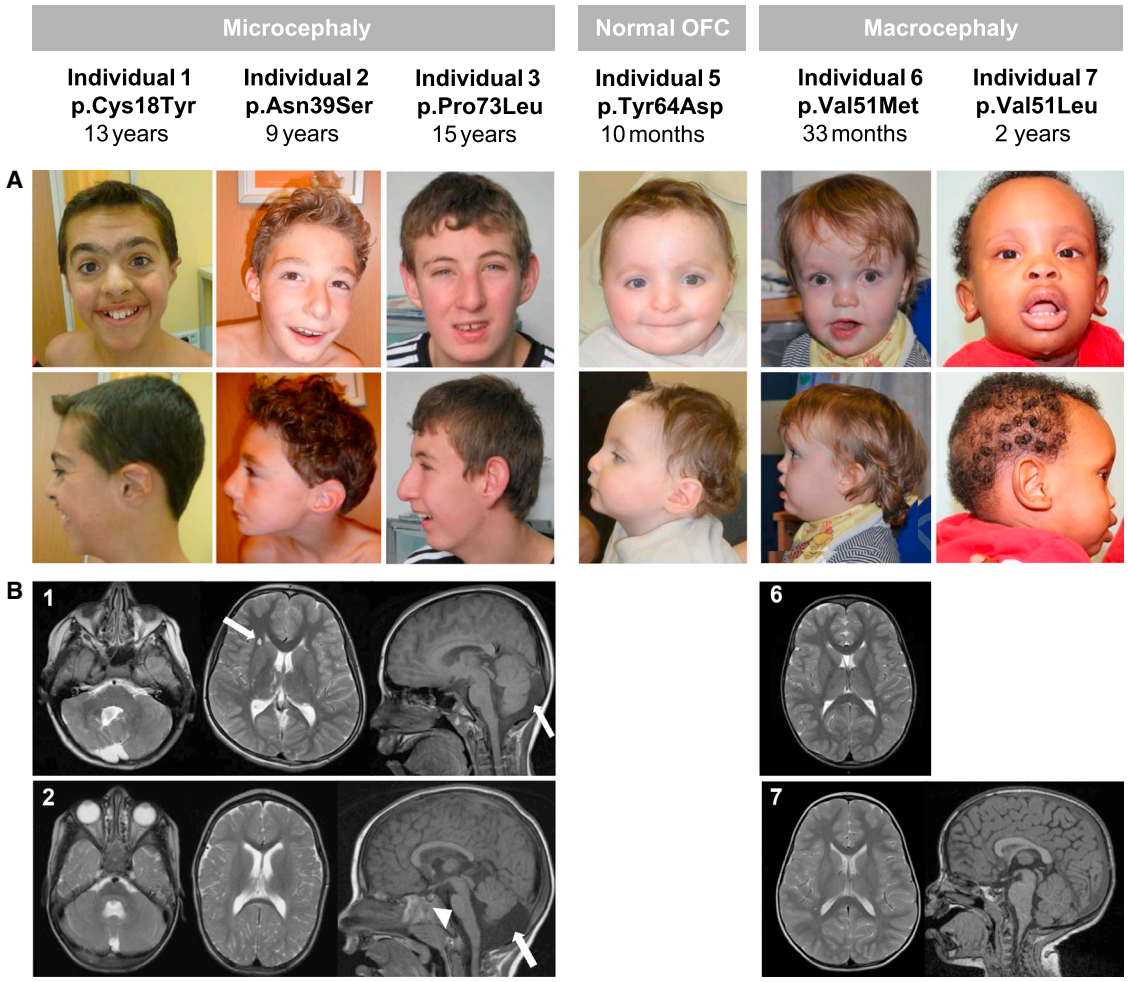

Figure 2. Facial Dysmorphism and Brain Abnormalities Observed in Individuals with *RAC1* Mutations
(A) Frontal and lateral photographs of the faces of individuals 1–3 and 5–7. Individuals 1, 2, and 3 were microcephalic, individual 5 had a normal occipital-frontal circumference, and individuals 6 and 7 had macrocephaly. Variable degrees of arched eyebrows, dysplastic ears, prominent nasal bridge, and overhanging columella were noted. Individuals with macrocephaly have prominent broad foreheads, slightly up-slanted palpebral fissures, open mouths, and "scooped out" appearance on lateral view.
(B) Panel 1 shows brain MRI images of individual 1: axial T2 images showing dysgenetic vermis and right cerebellar hemisphere (left), cystis lesions in the right frontal deep white matter (middle, arrow), and sagittal T1 images (right) showing enlarged cisterna magna (arrow). Panel 2 shows brain MRI images of individual 2: axial T2 images showing hypoplastic cerebellar vermis (left), slightly enlarged lateral ventricles (middle), and sagittal T1 images (right) showing hypoplastic corpus callosum, pons (arrow head), hypoplastic lower vermis, enlarged 4th ventricle, and cisterna magna (arrow). Panel 6 shows brain MRI image of individual 6: axial T2 image showing non-specific white matter changes in the frontal and parietal lobes. No hydrocephalus or extra-axial fluid was observed. Panel 7 shows brain MRI of individual 7: T2 weighted MRI images. Left: axial image showing very discrete bilateral patchy high intensity signal changes in the deep white matter of the frontal and parietal lobes; right: mid-sagittal section showing, except for megalencephaly, normal brain structures.

methanol, 20% DMSO) at 4°C. The embryos were first rehydrated in progressively decreasing methanol solutions, bleached with 10% H_2O_2, 0.5% KOH, and 0.1% Triton-X. After two washes in PBS, the tissue was permeabilized with proteinase K followed by post-fixation with 4% PFA. PFA-fixed embryos were washed first in PBS and subsequently in IF buffer (0.1% Tween-20, 1% BSA in PBS) for 10 min at room temperature. The embryos were incubated in the blocking buffer (10% FBS, 1% BSA in PBS) for 1 hr at room temperature. After two washes in IF buffer for 10 min each, embryos were incubated overnight at 4°C with 1:500 phospho histone 3 (PH3, a marker for proliferating cells) primary antibody (ser10)-R (sc-8656-R, rabbit, Santa Cruz) in blocking solution. After two additional washes in IF buffer for 10 min each, embryos were incubated in the secondary antibody solution (Alexa Fluor goat anti-mouse IgG [A21207, Invitrogen] and donkey anti-rabbit [A21206, Invitrogen], 1:1,000) in blocking solution for 1 hr at room temperature. Proliferating cells were quantified by counting all positive cells on a dorsal view of a 48 hpf embryos, excluding the eyes from the scored area, using the ITCN ImageJ plugin that counts cells with 10 pixel width and 5 pixel minimum distance between them in order to be considered as separate cells. Statistical

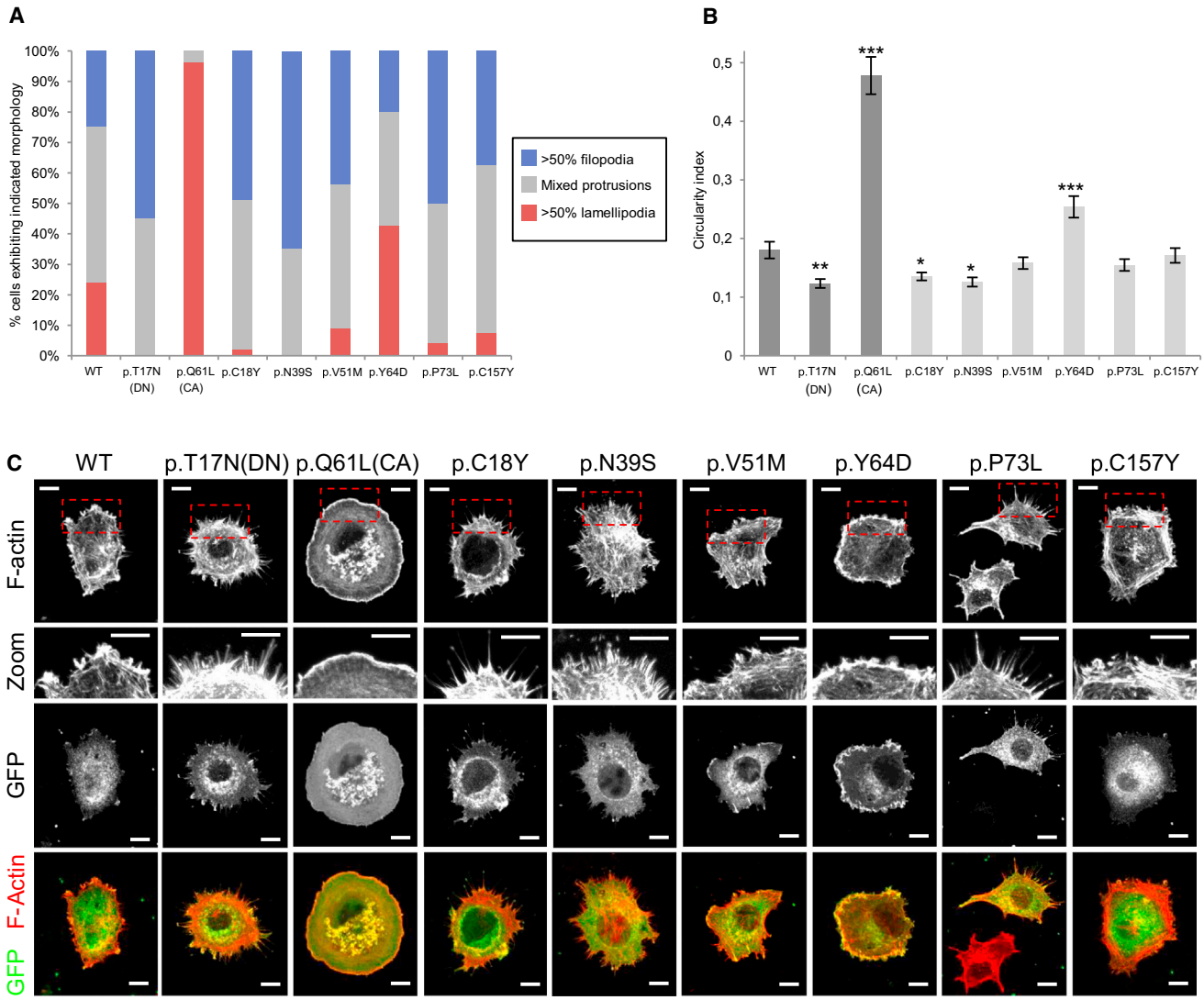

Figure 3. Distinct *RAC1* Mutations Genocopy Dominant-Negative or Constitutively Active Variants

(A) NIH 3T3 fibroblasts transfected with 500 ng of DNA per coverslip expressing the indicated Rac1 mutants and were fixed 30 min after plating onto fibronectin and stained with Alexa-568 phalloidin to reveal the actin cytoskeleton and anti-GFP to reveal the expressed construct. Cells were imaged by confocal microscopy and divided into the three indicated categories. At least 50 cells were analyzed for each dataset except p.Asn39Ser, p.Tyr64Asp, p.Cys157Tyr (40 cells), and p.Gln61Leu (25 cells). Data were pooled from three independent experiments.

(B) Graph showing mean circularity index of cells expressing indicated Rac1 mutants. Error bars indicate SEM. Datasets statistically analyzed using ANOVA test with Dunnett's correction for multiple comparisons. Asterisks indicate datasets significantly different to WT (*$p < 0.05$, **$p < 0.01$, ***$p < 0.001$).

(C) Images of cells expressing the indicated RAC1 mutation. In each case the cell is a representative example of the most common morphological category for that mutation (see A). Top panels show Alexa-568 phalloidin staining to reveal F-actin distribution, while the panels immediately below show a magnified view of the boxed region from the top panels to highlight the morphology of actin protrusions at the cell periphery. The third row of panels show the GFP channel of the same cells to reveal the distribution of the expressed RAC1 mutation, and the bottom panels show a merge of the F-actin (red) and GFP (green) channels. All scale bars indicate 10 μm.

significance for this assay was established using Student's t test. This assay showed significantly reduced cellular proliferation for both mutants ($p = 0.0012$ for p.Cys18Tyr and $p = 0.0018$ for p.Asn39Ser when compared to WT *RAC1*; Figures 4C and 4D).

Finally, armed with prior knowledge that RAC1 has a known role in cerebellar development[36] together with the observation that cerebellar abnormalities were reported in 3/7 individuals in our cohort, we sought to study the effect of the p.Cys18Tyr and p.Asn39Ser variants on cerebellar development of our zebrafish model. For the assessment of the cerebellum, embryos were fixed at 72 hpf in Dent's fixative and subsequently whole-mount stained following the same staining protocol as for neuronal proliferation and using a primary antibody against acetylated tubulin (1:1,000; Thr7451, mouse,

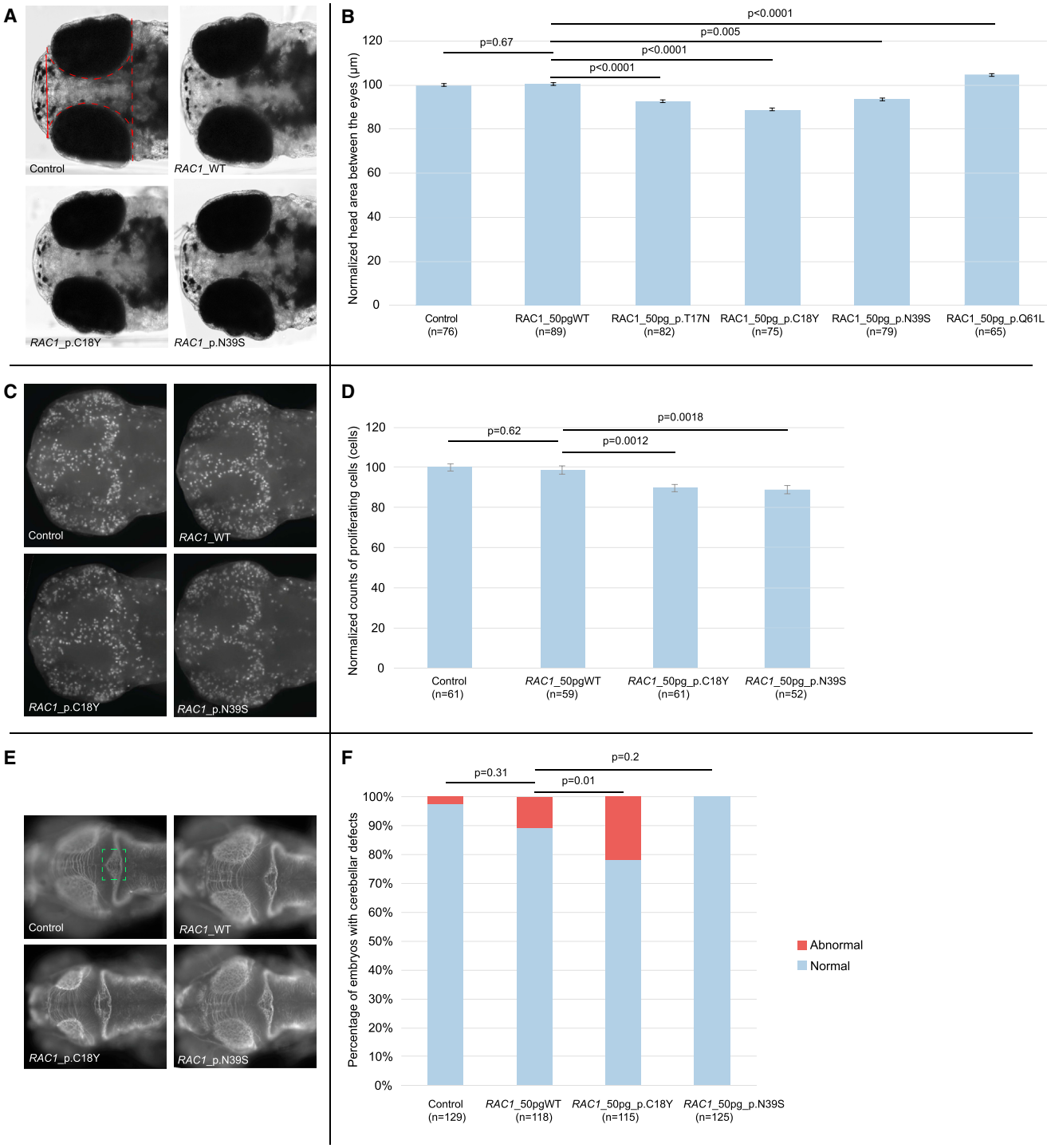

Figure 4. Overexpression of Human RAC1 p.Cys18Tyr and p.Asn39Ser Cause Microcephaly, while p.Gln61Leu Causes the Mirror Phenotype in Zebrafish Embryos

Functional assessment of *de novo* variants in *RAC1* by *in vivo* complementation in zebrafish larvae.

(A) Dorsal view of 5 days post fertilization (dpf) control and overexpressant larvae. For each experiment, embryos were injected with either WT or mutant *RAC1* human mRNA message. The embryos were allowed to grow to 5 dpf and imaged live for head size. The midbrain area between the eyes highlighted with the dashed red line was measured for every imaged embryo, to produce a quantitative score.

(B) Bar graph of normalized values showing the quantification of the head size phenotype in control embryos and embryos injected with either WT or mutant human *RAC1* message, from two plotted experiments. Statistical analyses were performed by Student's t test.

(C) Dorsal view of 2 dpf control and overexpressant larvae, fixed in Dent's fixative and whole-mount immuno-stained with an anti-phospho histone 3 (PH3) antibody that marks proliferating cells. For each experiment, embryos were injected with either WT or mutant *RAC1* human mRNA message. The embryos were allowed to grow to 2 dpf and subsequently were fixed, stained, and imaged. Embryos were imaged dorsally and z stacks were acquired every 100 nm. The z stacks were collapsed to produce an extended depth of focus (EDF) image

(legend continued on next page)

Sigma-Aldrich). The embryos were then scored qualitatively assaying the integrity of the cerebellum by scoring for the presence and organization of axons along the midline of the structure (highlighted with a green dashed box; Figure 4E) and statistical significance was determined using a χ^2 test. Structural defects in the integrity of the cerebellum consisted of depletion of the axons that cross the midline were observed only upon overexpression of *RAC1* p.Cys18Tyr ($p = 0.01$) but not *RAC1* p.Asn39Ser ($p = 0.2$) (Figures 4E and 4F). The latter is likely consistent with the more pronounced cerebellar defect observed in individual 1 (who harbors the p.Cys18Tyr variant) (Figure 2B).

In summary, we report seven individuals with *de novo* missense *RAC1* mutations and variable developmental delay with additional features. Remarkably, the OCFs observed in this study ranged from −5 SD to +4.5 SD. Previously, some chromosomal regions have been associated with both microcephaly (deletions) and macrocephaly (duplications).[37–39] However, it is extremely rare that point mutations within the same gene can cause differences of such magnitude (~10 SD) in head size of affected individuals. It is interesting to note that RAC1 is involved in mTOR signaling and other disorders in this pathway also result in significant alterations in head size.[17,40,41] The variability of RAC1 phenotypes appear to be dependent on specific mutations, although the contribution of genetic background cannot be ruled out. In silico modeling, mouse fibroblasts spreading assays, and zebrafish experiments demonstrate that some *RAC1* mutations (those encoding p.Cys18Tyr and p.Asn39Ser) genocopy a known dominant-negative mutant (p.Thr17Asn) and result in reduced neuronal proliferation, microcephaly, and cerebellar abnormalities *in vivo*. On the other hand, the *in vitro* effects of p.Tyr64Asp, seen in affected individual 5 with OFC within the normal range, are similar to the known constitutively active *RAC1* mutation. Of note, *in vitro* expression of dominant-negative and constitutively active *Rac1* have been previously shown to cause opposite effects on dendritic growth and morphology.[18] However, the link between the human mutations and the resultant phenotypes is likely to be complex depending on the balance between interactors, regulators, and effectors of RAC1 signaling.[42] This is likely to be especially true for other *RAC1* mutations identified in this study that could not be clearly classed as being either dominant negative or constitutively active (those encoding p.Val51Met, p.Pro73Leu, and p.Cys157Tyr). Further studies will be required in the future to uncover the precise underlying mechanisms of phenotypic variability of *RAC1* mutations.

Our findings show that mutations in genes encoding members of the RhoGTPases-family can cause DDs. Of note, mutations in *TRIO* (MIM: 601893), a gene that encodes a RAC1 GEF, have been shown to result in mild intellectual disability.[43,44] Interestingly, missense mutations in RAC-GEF domain of *TRIO* result in a more severe phenotype with global developmental delay, microcephaly, and reduced RAC1 activity.[43] Furthermore, biallelic mutations in *HACE1* (MIM: 610876), a known interactor of RAC1, have been recently shown to result in an autosomal-recessive syndrome with macrocephaly.[45] Notably, overexpression of a WAVE mutant has been demonstrated to partially rescue axon growth in *Rac1* knock-out neurons,[19] suggesting that some of the conditions in this group could be potentially treatable. Overall, a potentially treatable sub-category of rare DDs appears to be emerging with RAC1 as the central player.

Finally, our results show that ultra-rare disorders caused by private, non-recurrent missense mutations, resulting in varying phenotypic effects severity and degrees of severity, are challenging to dissect but can be delineated through focused international collaborations.

Supplemental Data

Supplemental Data include Supplemental Note and three figures and can be found with this article online at http://dx.doi.org/10.1016/j.ajhg.2017.08.007.

Acknowledgments

We would like to thank all the families for agreeing to participate in this study. We acknowledge the Rare Disease Foundation and the BC Children's Hospital Foundation for their support for this work (S.B., grant number 17-48). N.K. is a Distinguished George W. Brumley Professor. W.W.Y. is a researcher at the Structural Genomics Consortium, a registered charity (number 1097737; funding details online). We thank Prof. Viki Allan (University of Manchester) for providing mammalian expression plasmids encoding GFP-Rac1, GFP-Rac1-T17N, and GFP-Rac1-Q61L. The DDD study presents independent research commissioned by the Health Innovation Challenge Fund (grant number HICF-1009-003), a parallel funding partnership between the Wellcome Trust and the Department of Health, and the Wellcome Trust Sanger

that was then processed for scoring. The PH3-positive cells were counted for every embryo imaged using the ITCN plugin from ImageJ, to produce a quantitative score.
(D) Bar graph of normalized values showing the quantification of the proliferating cell count phenotype, across three biological replicas. Statistical analyses for the neuronal proliferation experiments were performed by Student's t test.
(E) Dorsal view of 3 dpf control and overexpressant larvae for *RAC1* WT and mutant conditions. The area of the cerebellum consisting of the neuronal axons that cross the midline is highlighted with a green dashed box. At least 50 embryos per condition were imaged live and evaluated at 3 dpf for the depletion of axons within the area highlighted.
(F) Bar graph of cumulative plotted experiments across three biological replicas showing percentages of embryos with cerebellar defects. Statistical analyses for the cerebellar integrity assay using a χ^2 test.
Error bars define 95% confidence interval.

Institute (grant number WT098051). The views expressed in this publication are those of the author(s) and not necessarily those of the Wellcome Trust or the Department of Health. The study has UK Research Ethics Committee approval (10/H0305/83 granted by the Cambridge South REC and GEN/284/12 granted by the Republic of Ireland REC). The research team acknowledges the support of the National Institute for Health Research, through the Comprehensive Clinical Research Network.

Received: April 4, 2017
Accepted: August 1, 2017
Published: September 7, 2017

Web Resources

ExAC Browser, http://exac.broadinstitute.org/gene/ENSG00000136238
GenBank, http://www.ncbi.nlm.nih.gov/genbank/
ImageJ, https://imagej.nih.gov/ij/
Molsoft, http://www.molsoft.com/icm_pro.html
OMIM, http://www.omim.org/
RCSB Protein Data Bank, http://www.rcsb.org/pdb/home/home.do
Structural Genomics Consortium, http://www.thesgc.org/

References

1. Sheridan, E., Wright, J., Small, N., Corry, P.C., Oddie, S., Whibley, C., Petherick, E.S., Malik, T., Pawson, N., McKinney, P.A., and Parslow, R.C. (2013). Risk factors for congenital anomaly in a multiethnic birth cohort: an analysis of the Born in Bradford study. Lancet *382*, 1350–1359.
2. Ropers, H.H. (2010). Genetics of early onset cognitive impairment. Annu. Rev. Genomics Hum. Genet. *11*, 161–187.
3. Deciphering Developmental Disorders Study (2017). Prevalence and architecture of de novo mutations in developmental disorders. Nature *542*, 433–438.
4. Iossifov, I., O'Roak, B.J., Sanders, S.J., Ronemus, M., Krumm, N., Levy, D., Stessman, H.A., Witherspoon, K.T., Vives, L., Patterson, K.E., et al. (2014). The contribution of de novo coding mutations to autism spectrum disorder. Nature *515*, 216–221.
5. Deciphering Developmental Disorders Study (2015). Large-scale discovery of novel genetic causes of developmental disorders. Nature *519*, 223–228.
6. Lelieveld, S.H., Reijnders, M.R., Pfundt, R., Yntema, H.G., Kamsteeg, E.J., de Vries, P., de Vries, B.B., Willemsen, M.H., Kleefstra, T., Löhner, K., et al. (2016). Meta-analysis of 2,104 trios provides support for 10 new genes for intellectual disability. Nat. Neurosci. *19*, 1194–1196.
7. MacArthur, D.G., Manolio, T.A., Dimmock, D.P., Rehm, H.L., Shendure, J., Abecasis, G.R., Adams, D.R., Altman, R.B., Antonarakis, S.E., Ashley, E.A., et al. (2014). Guidelines for investigating causality of sequence variants in human disease. Nature *508*, 469–476.
8. Rauen, K.A. (2013). The RASopathies. Annu. Rev. Genomics Hum. Genet. *14*, 355–369.
9. Van Aelst, L., and D'Souza-Schorey, C. (1997). Rho GTPases and signaling networks. Genes Dev. *11*, 2295–2322.
10. Heasman, S.J., and Ridley, A.J. (2008). Mammalian Rho GTPases: new insights into their functions from in vivo studies. Nat. Rev. Mol. Cell Biol. *9*, 690–701.
11. Duquette, P.M., and Lamarche-Vane, N. (2014). Rho GTPases in embryonic development. Small GTPases *5*, 8.
12. Stankiewicz, T.R., and Linseman, D.A. (2014). Rho family GTPases: key players in neuronal development, neuronal survival, and neurodegeneration. Front. Cell. Neurosci. *8*, 314.
13. Aspenström, P., Fransson, A., and Saras, J. (2004). Rho GTPases have diverse effects on the organization of the actin filament system. Biochem. J. *377*, 327–337.
14. Boureux, A., Vignal, E., Faure, S., and Fort, P. (2007). Evolution of the Rho family of ras-like GTPases in eukaryotes. Mol. Biol. Evol. *24*, 203–216.
15. Tahirovic, S., Hellal, F., Neukirchen, D., Hindges, R., Garvalov, B.K., Flynn, K.C., Stradal, T.E., Chrostek-Grashoff, A., Brakebusch, C., and Bradke, F. (2010). Rac1 regulates neuronal polarization through the WAVE complex. J. Neurosci. *30*, 6930–6943.
16. Wojnacki, J., Quassollo, G., Marzolo, M.P., and Cáceres, A. (2014). Rho GTPases at the crossroad of signaling networks in mammals: impact of Rho-GTPases on microtubule organization and dynamics. Small GTPases *5*, e28430.
17. Saci, A., Cantley, L.C., and Carpenter, C.L. (2011). Rac1 regulates the activity of mTORC1 and mTORC2 and controls cellular size. Mol. Cell *42*, 50–61.
18. Sugihara, K., Nakatsuji, N., Nakamura, K., Nakao, K., Hashimoto, R., Otani, H., Sakagami, H., Kondo, H., Nozawa, S., Aiba, A., and Katsuki, M. (1998). Rac1 is required for the formation of three germ layers during gastrulation. Oncogene *17*, 3427–3433.
19. Threadgill, R., Bobb, K., and Ghosh, A. (1997). Regulation of dendritic growth and remodeling by Rho, Rac, and Cdc42. Neuron *19*, 625–634.
20. Leone, D.P., Srinivasan, K., Brakebusch, C., and McConnell, S.K. (2010). The rho GTPase Rac1 is required for proliferation and survival of progenitors in the developing forebrain. Dev. Neurobiol. *70*, 659–678.
21. Chen, L., Melendez, J., Campbell, K., Kuan, C.Y., and Zheng, Y. (2009). Rac1 deficiency in the forebrain results in neural progenitor reduction and microcephaly. Dev. Biol. *325*, 162–170.
22. Sobreira, N., Schiettecatte, F., Valle, D., and Hamosh, A. (2015). GeneMatcher: a matching tool for connecting investigators with an interest in the same gene. Hum. Mutat. *36*, 928–930.
23. Matos, P., Skaug, J., Marques, B., Beck, S., Veríssimo, F., Gespach, C., Boavida, M.G., Scherer, S.W., and Jordan, P. (2000). Small GTPase Rac1: structure, localization, and expression of the human gene. Biochem. Biophys. Res. Commun. *277*, 741–751.
24. Lek, M., Karczewski, K.J., Minikel, E.V., Samocha, K.E., Banks, E., Fennell, T., O'Donnell-Luria, A.H., Ware, J.S., Hill, A.J., Cummings, B.B., et al.; Exome Aggregation Consortium (2016). Analysis of protein-coding genetic variation in 60,706 humans. Nature *536*, 285–291.
25. Jordan, P., Brazåo, R., Boavida, M.G., Gespach, C., and Chastre, E. (1999). Cloning of a novel human Rac1b splice variant with increased expression in colorectal tumors. Oncogene *18*, 6835–6839.
26. Colicelli, J. (2004). Human RAS superfamily proteins and related GTPases. Sci. STKE *2004*, RE13.
27. Hobbs, G.A., Mitchell, L.E., Arrington, M.E., Gunawardena, H.P., DeCristo, M.J., Loeser, R.F., Chen, X., Cox, A.D., and Campbell, S.L. (2015). Redox regulation of Rac1 by thiol oxidation. Free Radic. Biol. Med. *79*, 237–250.

28. Gao, Y., Xing, J., Streuli, M., Leto, T.L., and Zheng, Y. (2001). Trp(56) of rac1 specifies interaction with a subset of guanine nucleotide exchange factors. J. Biol. Chem. *276*, 47530–47541.
29. De Baets, G., Van Durme, J., Reumers, J., Maurer-Stroh, S., Vanhee, P., Dopazo, J., Schymkowitz, J., and Rousseau, F. (2012). SNPeffect 4.0: on-line prediction of molecular and structural effects of protein-coding variants. Nucleic Acids Res. *40*, D935–D939.
30. Price, L.S., Leng, J., Schwartz, M.A., and Bokoch, G.M. (1998). Activation of Rac and Cdc42 by integrins mediates cell spreading. Mol. Biol. Cell *9*, 1863–1871.
31. Ridley, A.J., Paterson, H.F., Johnston, C.L., Diekmann, D., and Hall, A. (1992). The small GTP-binding protein rac regulates growth factor-induced membrane ruffling. Cell *70*, 401–410.
32. Machesky, L.M., and Hall, A. (1997). Role of actin polymerization and adhesion to extracellular matrix in Rac- and Rho-induced cytoskeletal reorganization. J. Cell Biol. *138*, 913–926.
33. Michiels, F., Habets, G.G., Stam, J.C., van der Kammen, R.A., and Collard, J.G. (1995). A role for Rac in Tiam1-induced membrane ruffling and invasion. Nature *375*, 338–340.
34. Jao, L.E., Wente, S.R., and Chen, W. (2013). Efficient multiplex biallelic zebrafish genome editing using a CRISPR nuclease system. Proc. Natl. Acad. Sci. USA *110*, 13904–13909.
35. Perles, Z., Moon, S., Ta-Shma, A., Yaacov, B., Francescatto, L., Edvardson, S., Rein, A.J., Elpeleg, O., and Katsanis, N. (2015). A human laterality disorder caused by a homozygous deleterious mutation in MMP21. J. Med. Genet. *52*, 840–847.
36. Mulherkar, S., Uddin, M.D., Couvillon, A.D., Sillitoe, R.V., and Tolias, K.F. (2014). The small GTPases RhoA and Rac1 regulate cerebellar development by controlling cell morphogenesis, migration and foliation. Dev. Biol. *394*, 39–53.
37. Nevado, J., Rosenfeld, J.A., Mena, R., Palomares-Bralo, M., Vallespín, E., Ángeles Mori, M., Tenorio, J.A., Gripp, K.W., Denenberg, E., Del Campo, M., et al. (2015). PIAS4 is associated with macro/microcephaly in the novel interstitial 19p13.3 microdeletion/microduplication syndrome. Eur. J. Hum. Genet. *23*, 1615–1626.
38. Van Dijck, A., van der Werf, I.M., Reyniers, E., Scheers, S., Azage, M., Siefkas, K., Van der Aa, N., Lacroix, A., Rosenfeld, J., Argiropoulos, B., et al. (2015). Five patients with a chromosome 1q21.1 triplication show macrocephaly, increased weight and facial similarities. Eur. J. Med. Genet. *58*, 503–508.
39. Shinawi, M., Liu, P., Kang, S.H., Shen, J., Belmont, J.W., Scott, D.A., Probst, F.J., Craigen, W.J., Graham, B.H., Pursley, A., et al. (2010). Recurrent reciprocal 16p11.2 rearrangements associated with global developmental delay, behavioural problems, dysmorphism, epilepsy, and abnormal head size. J. Med. Genet. *47*, 332–341.
40. Rivière, J.B., Mirzaa, G.M., O'Roak, B.J., Beddaoui, M., Alcantara, D., Conway, R.L., St-Onge, J., Schwartzentruber, J.A., Gripp, K.W., Nikkel, S.M., et al.; Finding of Rare Disease Genes (FORGE) Canada Consortium (2012). De novo germline and postzygotic mutations in AKT3, PIK3R2 and PIK3CA cause a spectrum of related megalencephaly syndromes. Nat. Genet. *44*, 934–940.
41. Rosner, M., Hanneder, M., Siegel, N., Valli, A., Fuchs, C., and Hengstschläger, M. (2008). The mTOR pathway and its role in human genetic diseases. Mutat. Res. *659*, 284–292.
42. Hetmanski, J.H.R., Schwartz, J.M., and Caswell, P.T. (2016). Rationalizing Rac1 and RhoA GTPase signaling: A mathematical approach. Small GTPases, 1–6.
43. Pengelly, R.J., Greville-Heygate, S., Schmidt, S., Seaby, E.G., Jabalameli, M.R., Mehta, S.G., Parker, M.J., Goudie, D., Fagotto-Kaufmann, C., Mercer, C., et al.; DDD Study (2016). Mutations specific to the Rac-GEF domain of TRIO cause intellectual disability and microcephaly. J. Med. Genet., jmedgenet-2016-103942.
44. Ba, W., Yan, Y., Reijnders, M.R., Schuurs-Hoeijmakers, J.H., Feenstra, I., Bongers, E.M., Bosch, D.G., De Leeuw, N., Pfundt, R., Gilissen, C., et al. (2016). TRIO loss of function is associated with mild intellectual disability and affects dendritic branching and synapse function. Hum. Mol. Genet. *25*, 892–902.
45. Hollstein, R., Parry, D.A., Nalbach, L., Logan, C.V., Strom, T.M., Hartill, V.L., Carr, I.M., Korenke, G.C., Uppal, S., Ahmed, M., et al. (2015). HACE1 deficiency causes an autosomal recessive neurodevelopmental syndrome. J. Med. Genet. *52*, 797–803.

The American Journal of Human Genetics, Volume *101*

Supplemental Data

RAC1 Missense Mutations in Developmental Disorders with Diverse Phenotypes

Margot R.F. Reijnders, Nurhuda M. Ansor, Maria Kousi, Wyatt W. Yue, Perciliz L. Tan, Katie Clarkson, Jill Clayton-Smith, Ken Corning, Julie R. Jones, Wayne W.K. Lam, Grazia M.S. Mancini, Carlo Marcelis, Shehla Mohammed, Rolph Pfundt, Maian Roifman, Ronald Cohn, David Chitayat, Deciphering Developmental Disorders Study, Tom H. Millard, Nicholas Katsanis, Han G. Brunner, and Siddharth Banka

Supplemental Note: Case Reports

Individual 1 (male, 13 years) - He is the second of four children born to non-consanguineous parents. The mother is of Dutch ancestry and the father of Egyptian ancestry. Family history was non-contributory. He was born after uncomplicated pregnancy and delivery. He had neonatal feeding problems and an absent suck reflex. He walked without support at the age of 18 months and spoke his first words at the age of 6 years. Psychological assessment at the age of 13 years showed severe intellectual disability with an IQ of 35. He developed epilepsy at the age of 2 years. He has a progressive scoliosis that affected his mobility and required surgical correction. At 13 years of age, his height was 137 cm (-2.5 SD), weight was 30 kg (0 SD) and occipito-frontal circumference (OFC) was 50 cm (-2.5 SD). He has small and dysplastic ears, synophrys, arched eyebrows, long palpebral fissures, broad nasal tip, short philtrum and broad canine teeth. His hands and feet are small with bilateral simian creases, 5^{th} finger brachydactyly and hyperlaxity of joints. Magnetic resonance imaging (MRI) studies of the brain at the age of 12 years showed severe dysplasia of cerebellar vermis and right cerebellar hemisphere, large retrocerebellar arachnoid cyst, mega cisterna magna, hypoplasia of splenium of the corpus callosum, bilateral cystic lesions in the cerebral white matter: possibly small lacunar infarcts, multiple lesions in the deep white matter frontoparietal, mild dilatation of the posterior horn of the lateral ventricles. He has mild insufficiency of all four cardiac valves and non-synchronic left ventricular contractions. Previous investigation included normal metabolic screening in urine and blood, 250k SNP array and targeted sequencing for *TCF4*, *PTPN11* and *ANKRD11*. Whole exome sequencing (WES) revealed a heterozygous *de novo* mutation in *RAC1*: Chr7(GRCh37):g.6426860G>A; NM_018890.3:c.53G>A; p.(Cys18Tyr).

Individual 2 (male, 9 years) – He is the only child of non-consanguineous parents of Dutch ancestry. There was no family history of developmental delay. Pregnancy was complicated by pregnancy induced hypertension. He was born at 32 weeks and 4 days of gestation via a Caesarian section for fetal distress and intra-uterine growth retardation. He had frequent pneumonias and hyperbilirubinemia during infancy. Both motor and language development were delayed. Psychological assessment at the age of 7 years showed mild to moderate intellectual disability with an IQ of 51. He is hyperactive with poor attention and has a high pain threshold. He has a friendly personality. He has a history of constipation and frequent dental caries. At the age of 9 years his height was 128 cm (-1.5SD), weight was 24 kg (-0.5 SD) and OFC was 47.7 cm (-3 SD). He has low set, posteriorly rotated and dysplastic ears, full eyebrows, long palpebral fissures, broad nasal tip, flat philtrum, broad mouth and pointed chin. Brain MRI at the age of 2.5 years showed mildly enlarged lateral ventricles, hypoplastic pons , hypoplastic lower lobe of the cerebellar vermis, mega cisterna

magna, enlarged fourth ventricle, thin splenium and rostrum of the corpus callosum. Previous genetic investigations included normal karyotyping, analysis of subtelomeric regions and 250k SNP array. WES revealed a heterozygous *de novo* mutation in *RAC1*: Chr7(GRCh37):g.6431563A>G; NM_018890.3:c.116A>G p.(Asn39Ser).

Individual 3 (male, 15 years, DDD 260739) – He is born to non-consanguineous parents. Increased nuchal thickness was noted prenatally. He was born at 40 weeks of gestation. He was noted to have a poor suck and had neonatal feeding problems. His developmental milestones are not available. Currently, he has a few single words. At 15 years of age his OFC was 47 cm (-5 SD). Trio WES sequencing revealed a heterozygous *de novo* mutation in the *RAC1* gene Chr7(GRCh37):g.6431665C>T; NM_018890.3: c.218C>T p.(Pro73Leu).

Individual 4 (male, 6 months) – He is the first child of healthy non-consanguineous couple of French Canadian-Polish and Armenian descent. There was a family history of postaxial polydactyly of the feet in the maternal aunt and grandmother. Prenatal scans revealed multiple fetal abnormalities, including cerebellar hypoplasia, shortened corpus callosum, prominent cisterna magna, an echogenic intra-cardiac focus, hypertelorism, postaxial polydactyly on all four limbs, single umbilical artery, and near term onset of growth restriction. At birth, the baby was also found to have a large anterior fontanelle, flat nasal bridge, broad upturned nose, hypoplastic alae nasi, full lips, umbilical hernia, cryptorchidism and hypospadias. The baby was microcephalic at birth (with a head circumference at 2 SD below the mean); birth weight and length were within the normal range (both at the 30th centile). The boy required several days of respiratory support initially, and had recurrent apneic episodes in the first few months of life; consequent investigations revealed tracheobronchomalacia, central apnea and subclinical seizures. On assessment at 2 and 4 months of age, he had global developmental delay, central hypotonia, microcephaly (-2.5 SD) and poor weight gain (-3 SD). His length remained in the normal range (20th centile). Brain MRI showed abnormal cerebellar foliation, lower vermis hypoplasia, large supravermian cyst, mega cisterna magna, abnormal brainstem with loss of normal pontomedullary sulcation, and short corpus callosum with tapering of the posterior body and splenium. Echocardiogram revealed bicuspid aortic valve, patent foramen ovale and patent ductus arteriosus. Karyotype and 250k SNP-array were normal. WES revealed a heterozygous d*e novo* novel mutation in exon 7 of the *RAC1* gene: Chr7(GRCh37):g. 6441968G>A; NM_018890.3: c.470G>A p.(Cys157Tyr) and a maternally inherited novel variant of uncertain significance was also found in the *KIAA2022* gene (c.4228C>T; p.Pro1410Ser). While *KIAA2022* mutations are a known cause of X-linked mental retardation, the dysmorphic features and multiple anomalies found in this case do not fit the phenotype associated with mutations.[1; 2]

Individual 5 (male, 12y, DDD 265249) - is one of non-identical twins born to non-consanguineous parents. He was born at 38 weeks of gestation with a weight of 2.2 Kg (-2.17 SD). He was noted to be mildly hypotonic soon after birth. There is no history of neonatal feeding difficulties. He achieved social smile at 12 weeks of age. He has severe global developmental delay. He could sit without support from 19 months and can walk short distances with support from the age of 4 years. He does not have any expressive speech and his understanding is severely impaired. He has bilateral sensorineural hearing loss and mild visual impairment. He used to have head stereotypies as a young child but they have resolved. He has never had seizures but possibility of absences has been raised, although not proven. He was found to have a ventricular septal defect that was closed surgically at the age of 2 years. He has a small penis. His OFC at 8 years was 53 cm (0.07SD) and 56.5 cm (+1 SD) at 12 years of age. At 8 years his height was 134 cm (+1.03 SD). He has prominent metopic suture, wave-shaped palpebral fissures, a high palate, a prominent nasal bridge with low columella and dysplastic ears. A brain MRI at 2 years of age showed polymicrogyria. Previous testing included normal karyotype, Fragile X studies, urine metabolic screen, very long chain fatty acid levels, plasma lactate and SNP6 microarray. WES sequencing revealed a heterozygous *de novo* mutation in the *RAC1* gene Chr7(GRCh37):g.643163T>G; NM_018890.3: c.190T>G p.(Tyr64Asp).

Individual 6 (male, 33 months, DDD 270776) – He is the first child of non-consanguineous parents, who both have sensorineural hearing loss. The pregnancy was uneventful. The child was born at 39 weeks of gestation with a birth weight of 3.54 Kgs (0.42 SD). He has normal hearing. The birth OFC is not available but he was referred to Paediatrics at 4 months of age for macrophaly and his OFC at 11 months was 52cm (+1 SD). He was able to sit without support from 12 months and started walking independently between the ages of 2 and 2.5 years. At the age of 33 months his OFC was 56 cm (+4.16 SD). He has a prominent broad forehead, slightly up-slanted palpebral fissures, an open mouth and a 'scooped out' appearance on lateral view. A MRI brain scan at 12 months of age showed non-specific white matter change in the right frontal and parietal lobes in the peri-ventricular distribution. Previous genetic investigations included normal *PTEN* sequencing, array CGH, urine organic acids, white cell enzymes and Fragile X. WES revealed a heterozygous *de novo* mutation in *RAC1*: Chr7(GRCh37):g.6431598G>A; NM_018890.3: c.151G>A p.(Val51Met).

Individual 7 (male, 4 years and 5 months) – He is eldest of two children born to non-consanguineous parents of African American ancestry. Family history was negative for developmental delay and intellectual disability. The pregnancy was unremarkable, and the patient was born at term by spontaneous vaginal delivery. He had no perinatal problems. He was noted to have developmental

delay at 15 months of age when he was not crawling or walking and did not have any words at that time. He started having seizures at 1 year of age which were well controlled with Depakote. His EEG showed generalized cortical dysfunction and multifocal induced seizures. By 2 years of age he was walking but only had between 3 and 5 words which he used inconsistently. He is on the autistic spectrum. He has mild truncal hypotonia and symmetric hyporeflexia. He has a history of recurrent ear infections. He has significant eczema with associated hypopigmentation. At the age of 4 years 5 months his height was 109 cm (0 SD), weight was 23 kg (+2.5 SD) and OFC was 59.5 cm (+4.5 SD). He has a prominent broad forehead, up-slanted palpebral fissures, upturned ear lobes, an open mouth and a 'scooped out' appearance on lateral view. A brain MRI showed tiny punctate white matter lesions in the periventricular area. Previous testing included normal high resolution chromosomes, CytoScan microarray, plasma amino acids, urine organic acids, fragile X analysis, myotonic dystrophy analysis, *PTEN* sequencing, and a NGS lysosomal gene panel. Trio WES sequencing revealed a heterozygous *de novo* mutation in the *RAC1* gene Chr7(GRCh37):g.6431598G>C; NM_018890.3:c.151G>C p.(Val51Leu).

Supplemental figures and legends

Figure S1. Crystal structure of the RAC1-DOCK2 complex (PDB code 2YIN).

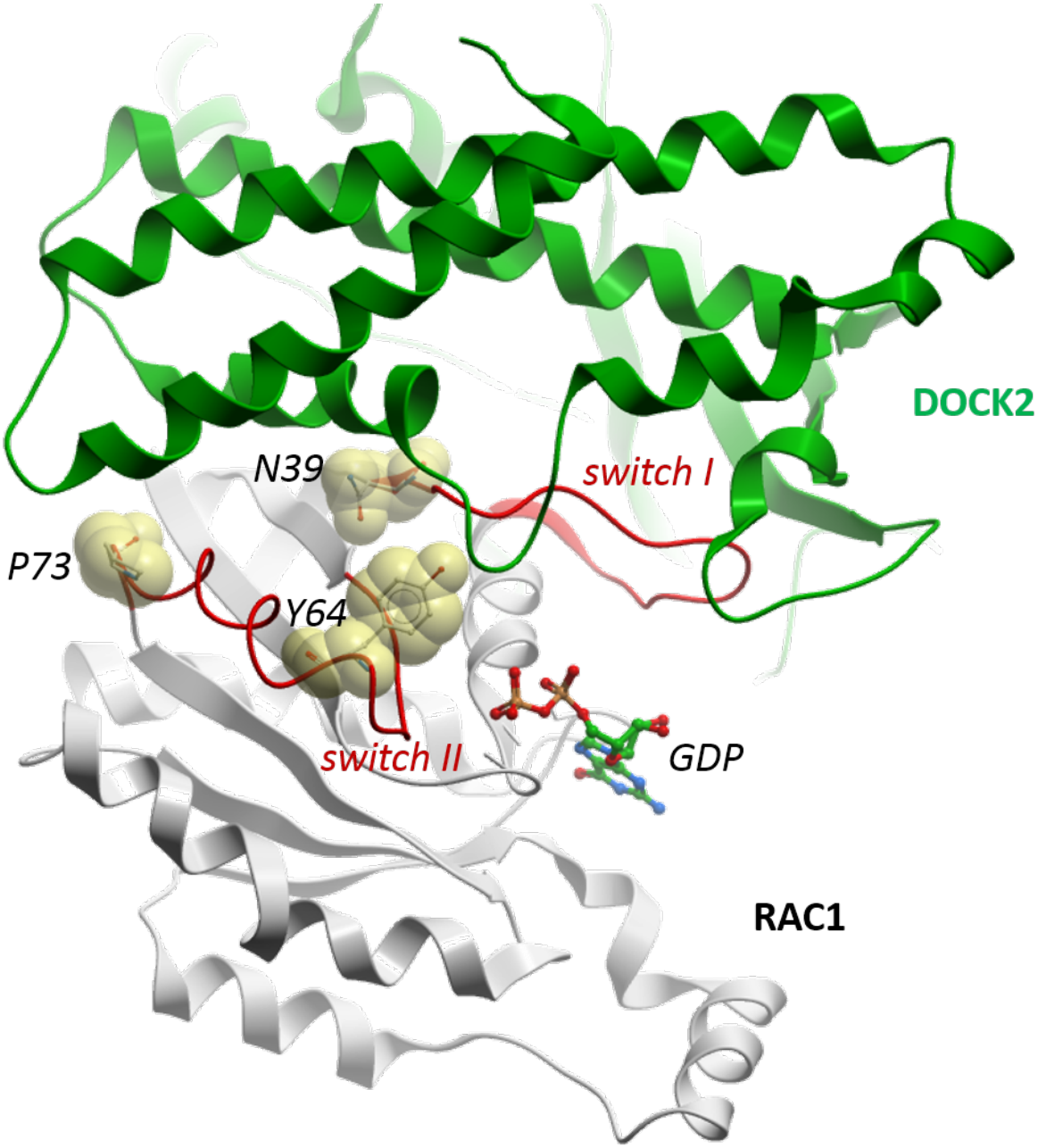

This figure highlights the use of Switch I and Switch II motifs (red) of RAC1 (grey cartoon) to interact with the guanine exchange factor DOCK2 (green cartoon). The three mutations predicted to affect this interaction are mapped onto RAC1 as spheres.

Figure S2. Evidence for the efficiency of the CRISPR reagent used to suppress the endogenous expression of *rac1* in developing zebrafish embryos.

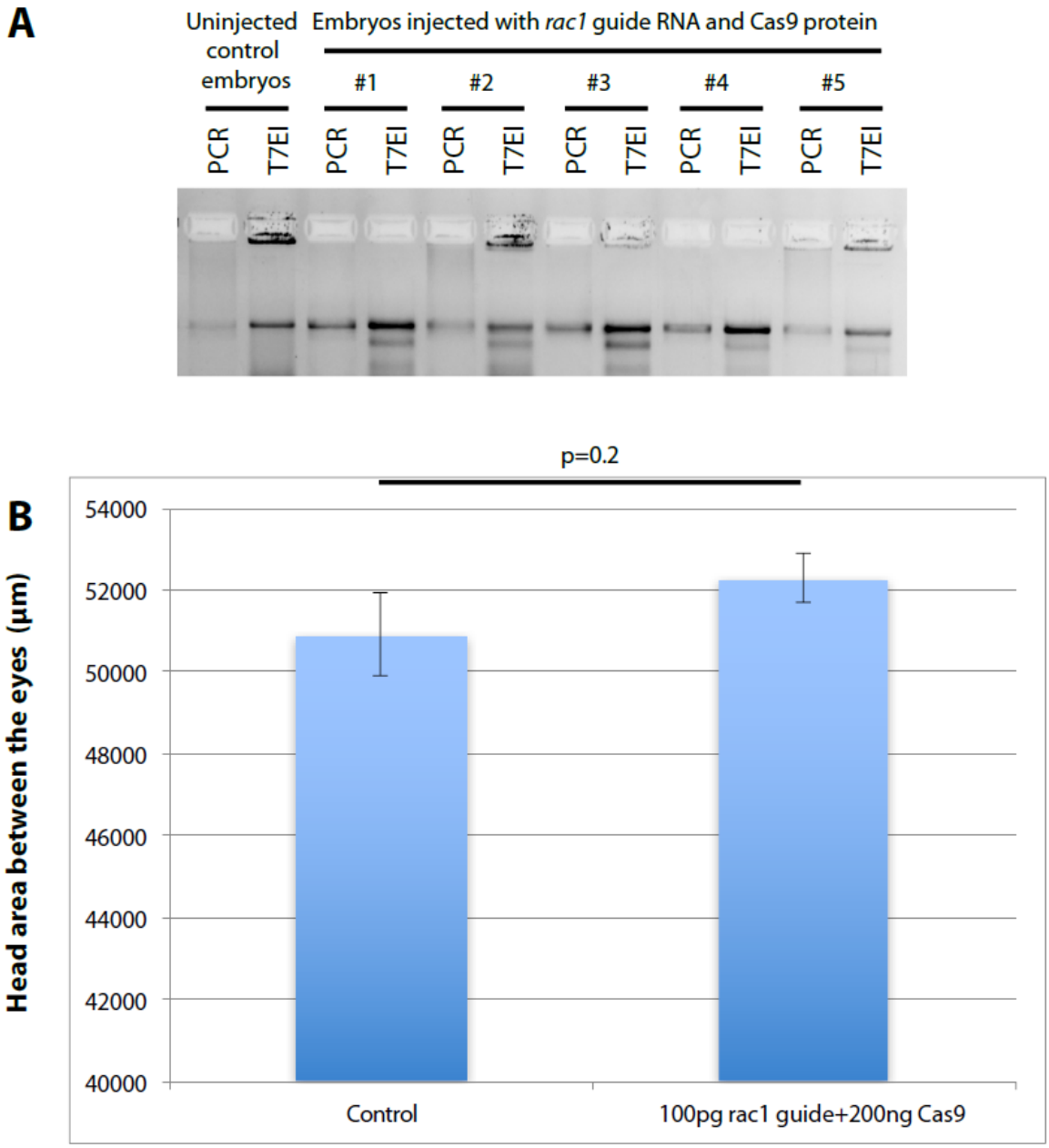

(A) For the cloning of the *rac1* guide template RNA was annealed the two oligonucleotides rac1_guide2_F: 5'-TAGGACCAGTAAACCTGGGATTGT-3' and rac1_guide2_R: 5'-AAACACAATCCCAGGTTTACTGGT-3'. The *rac1* guide oligonucleotide sequences were ligated into the pT7Cas9sgRNA vector (Addgene) using the *Bsm* BI sites. For the generation of the guide RNA, the template DNA was linearized with *Bam* HI, purified by phenol/chloroform extraction and *in vitro* transcribed using the MEGAshortscript T7 kit (Invitrogen). To generate F0 CRISPR mutants we injected 1nl containing 100pg *rac1* guide RNA and 200ng Cas9 protein (PNA bio, CP01) to 1-cell stage embryos. To determine the efficiency of the guide RNA, embryos were allowed to grow to 5dpf, at

which time they were euthanized and subjected to digestion with proteinase K (Life Technologies, AM2548) to extract genomic DNA. The targeted locus was PCR amplified using the drrac1_g2test_1F 5'-TCCCCAATTACATTTGTCATCA-3' and drrac1_g2test_1R 5'-ACTCATGGATATCGGCAAGC-3' primer pair. The PCR amplicons were subject to digestion using T7 endonuclease I (New England Biolabs, M0302L) at 37 °C for 1 hr and were visualized on a 2% agarose gel. For Sanger sequencing of individual products from the *rac1* locus, PCR fragments from four embryos with a positive T7assay were cloned into the pCR4/TOPO TA cloning vector (Life technologies, 450030) and 40 colonies from each cloned embryo were Sanger sequenced. Gel image showing the efficiency of the *rac1* guide RNA following T7 endonuclease assay evaluation. The first two lanes show control amplicons from the locus flanking the targeted sequence, with no aberrations observed. In the embryos injected with *rac1* guide RNA and Cas9 protein, aberrations are evident for embryos #1 - #5, showing that the guide efficiently introduced sequence aberrations in all injected embryos.

(B) Bar graph showing the quantification of the head size phenotype in control embryos and larvae injected with *rac1* guide RNA and Cas9. Statistical analyses were performed by student`s t-test.

Figure S3. Dose curve showing the effect of progressively increasing doses of WT *RAC1* in 5dpf zebrafish larvae.

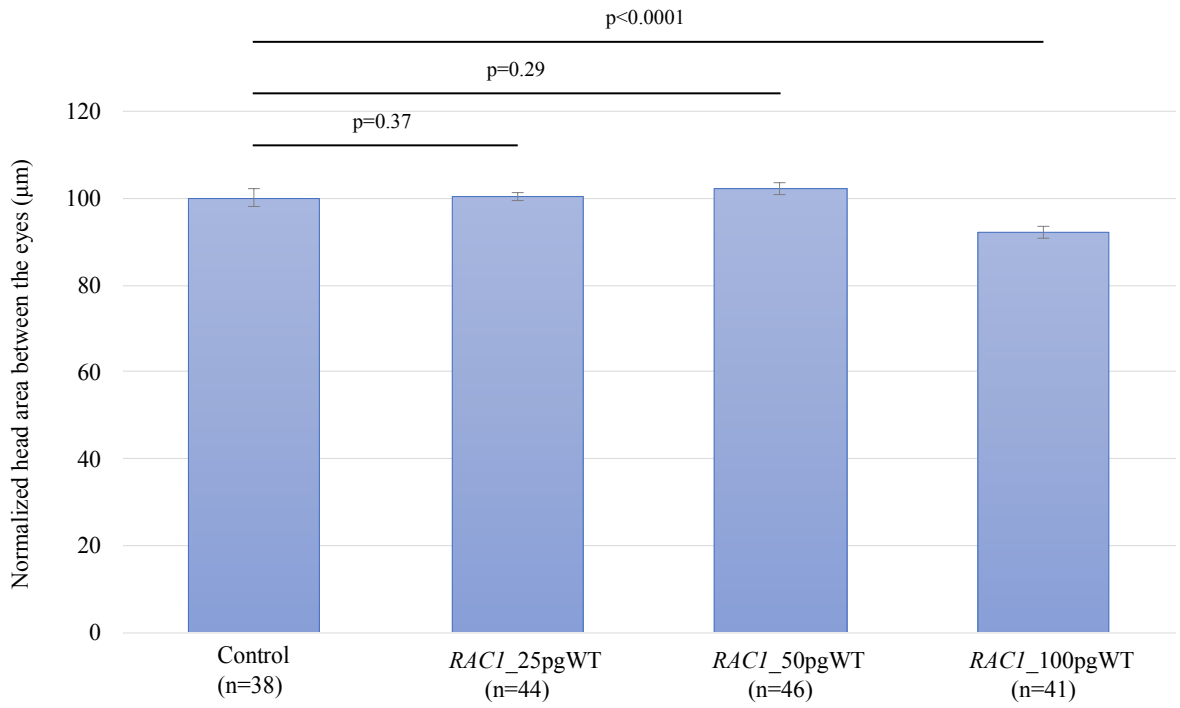

Bar graph showing the quantification of the head size phenotype in control embryos and embryos injected with progressively increasing doses of WT *RAC1* message. The bars represent cumulative normalized plotted experiments across two biological replicas. Statistical analyses were performed by student`s t-test.

Figure S4. The headsize phenotype caused by overexpression of d*e novo* mutations p.Cys18Tyr and p.Asn39Ser in *RAC1* cannot be antagonized by concomitant overexpression of WT *RAC1* message.

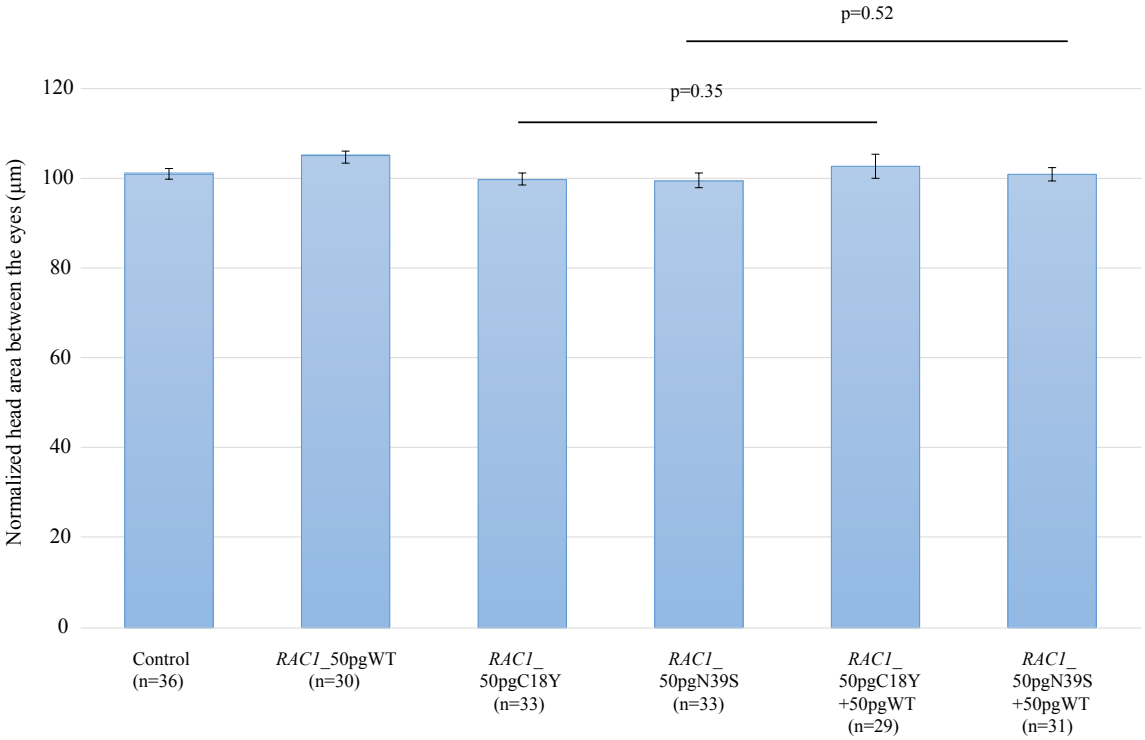

Bar graph showing the quantification of the head size phenotype in control embryos and embryos injected with WT, mutant or mutant + WT *RAC1* message. The bars represent normalized plotted experiments. Statistical analyses were performed by student`s t-test.

Supplemental references

1. Cantagrel, V., Lossi, A.M., Boulanger, S., Depetris, D., Mattei, M.G., Gecz, J., Schwartz, C.E., Van Maldergem, L., and Villard, L. (2004). Disruption of a new X linked gene highly expressed in brain in a family with two mentally retarded males. Journal of medical genetics 41, 736-742.
2. Van Maldergem, L., Hou, Q., Kalscheuer, V.M., Rio, M., Doco-Fenzy, M., Medeira, A., de Brouwer, A.P., Cabrol, C., Haas, S.A., Cacciagli, P., et al. (2013). Loss of function of KIAA2022 causes mild to severe intellectual disability with an autism spectrum disorder and impairs neurite outgrowth. Human molecular genetics 22, 3306-3314.